Reprinted from

JAPANESE JOURNAL OF
APPLIED
PHYSICS

REGULAR PAPER

Control of Thickness and Composition Variation of AlGaN/GaN on 6- and 8-in. Substrates Using Multiwafer High-Growth-Rate Metal Organic Chemical Vapor Deposition Tool

Yoshiki Yano, Hiroki Tokunaga, Hayato Shimamura, Yuya Yamaoka, Akinori Ubukata,
Toshiya Tabuchi, and Koh Matsumoto

Jpn. J. Appl. Phys. **52** (2013) 08JB06

Japanese Journal of Applied Physics **52** (2013) 08JB06 **REGULAR PAPER**
http://dx.doi.org/**10.7567/JJAP.52.08JB06**

Control of Thickness and Composition Variation of AlGaN/GaN on 6- and 8-in. Substrates Using Multiwafer High-Growth-Rate Metal Organic Chemical Vapor Deposition Tool

Yoshiki Yano[1*], Hiroki Tokunaga[1], Hayato Shimamura[2], Yuya Yamaoka[1], Akinori Ubukata[1], Toshiya Tabuchi[1], and Koh Matsumoto[2]

[1] *Taiyo Nippon Sanso Corporation, 10 Ohkubo, Tsukuba, Ibaraki 300-2611, Japan*
[2] *TN EMC Ltd., 2008-2 Wada, Tama-city, Tokyo 206-0001, Japan*
E-mail: Yoshiki.Yano@tn-sanso.co.jp

Received October 12, 2012; revised November 27, 2012; accepted December 2, 2012; published online May 20, 2013

It is difficult to control the surface temperature gradient over a bowing GaN on a large-diameter silicon substrate by metal organic chemical vapor deposition (MOCVD) because the wafer bows convexly to store compressive strain during growth. In an attempt to grow uniform AlGaN/GaN on 6-in. (6″) silicon substrates using a 7 × 6″ reactor, we described in this paper the control of the surface temperature gradient over the wafer and the mass transport at the edge of the wafer. We attempted to grow $Al_{0.23}GaN/AlN/GaN/SLS/Al_{0.5}GaN/AlN$ on six 8-in. (8″) silicon substrates using a 6 × 8″ reactor. The standard deviations of total thickness were less than 2.0% on wafer and 0.31% wafer to wafer. The growth rate of strained-layer superlattice (SLS) was as high as 2.8 μm/h. The typical electron mobility was 1670 $cm^2 \cdot V^{-1} \cdot s^{-1}$ at a sheet carrier density of 1.11 × 10^{13} cm^{-2}.

1. Introduction

There is considerable interest in the growth of GaN on silicon (Si) substrates because of its potential for low-cost, large size, and high-thermal-conductivity.[1–9] In recent years, high-performance GaN power devices have been demonstrated by other groups.[10–13] As is well known, there is a problem of the large difference in thermal expansion coefficient between GaN and Si in addition to the large lattice mismatch.[14] To solve the problem, it is necessary to induce compressive strain in a wafer during growth by employing an appropriate buffer layer structure. However, the temperature gradient over the wafer becomes larger because the wafer bows convexly during growth.[15] We also need a high growth rate of the buffer layer in order to obtain a high throughput.[16] To suppress hazardous parasitic reactions, which impede AlN and AlGaN growth, between organic metal and ammonia (NH_3), a high gas flow velocity is required.[17] However, a high gas flow velocity tends to induce a large temperature gradient in a wafer. Thus, we have developed tools for high-flow-velocity and high-growth-rate metal organic chemical vapor deposition (MOCVD) for mass production that can control vapor phase reactions.[18,19] In this paper, we describe the control of the surface temperature gradient over a bowing wafer by varying heater input power balance, and the growth of a uniform AlGaN layer over a 6-in. (6″) Si substrate by varying the flow balance between trilayer gas injection nozzle. We also describe a high-electron-mobility transistor (HEMT) structure on 8-in. (8″) Si substrates grown using our MOCVD tools.

2. Experiments

In this study, we used MOCVD reactors with capacities of 7 × 6″ (Taiyo Nippon Sanso UR25K) and 6 × 8″ or 10 × 6″ (UR26K) for mass production. These reactors were developed for LED and electron device manufacturing. Figure 1 shows the schematic of the reactors. The precursors and carrier gases are injected into the reaction zone from a trilayer nozzle at the center of these reactors. The nozzle is designed to introduce a high-velocity laminar flow in order to suppress hazardous parasitic reactions between an organic metal and ammonia (NH_3). The design criteria were described in our previous papers.[20,21] It is possible to control the growth rate at the edge by varying the flow rate balance of the carrier gases of the trilayer nozzle, as described in our previous papers.[22,23] All the wafers were rotated in a planetary motion. Wafer holders on the susceptor were heated by resistance heaters, which were controlled separately in six zones along the flow direction. Growth pressure was controlled by a variable conductance valve and a dry pump from 10 kPa to near atmospheric pressure. We adopted 13 kPa for AlN and AlGaN growth, and 13–90 kPa for GaN growth. The V/III ratios were about 190, 2000, and 3000 for AlN, AlGaN, and GaN, respectively. We used 150-mm-diameter (6″) 675-μm-thick and 200-mm-diameter (8″) 1-mm-thick Si(111) substrates. Trimethylgallium (TMG), trimethylaluminium (TMA), and NH_3 were used as the source gases of Ga, Al, and N, respectively. Hydrogen (H_2) and nitrogen (N_2) were also introduced as the carrier gases. The mapping of the epitaxial film thickness and Al composition of AlGaN was carried out by white light interference, photoluminescence (RPM-Σ), and X-ray diffraction (XRD) analyses. The thickness of each layer was

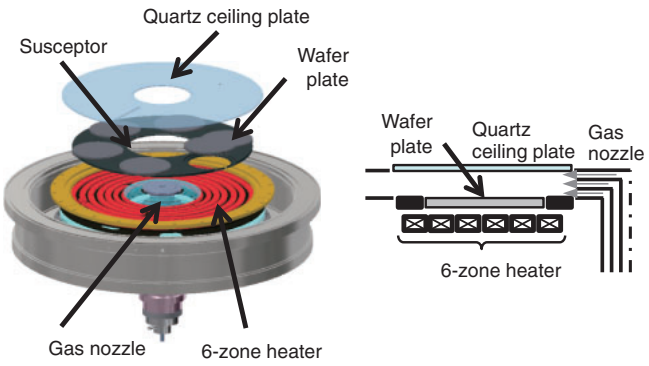

Fig. 1. (Color) Schematic of reactors (left figure) and sectional view of gas flow direction (right figure).

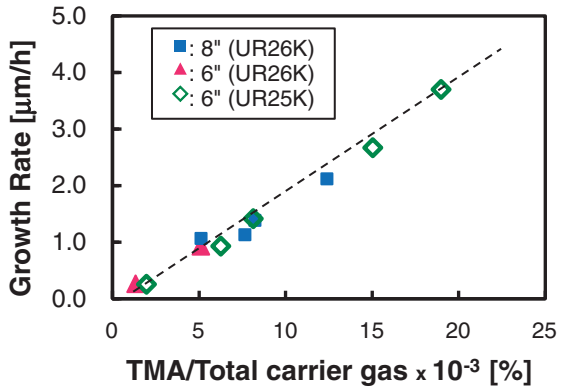

Fig. 2. (Color) AlN growth rate as function of TMA supply concentration for two different MOCVD reactors (UR25K and UR26K).

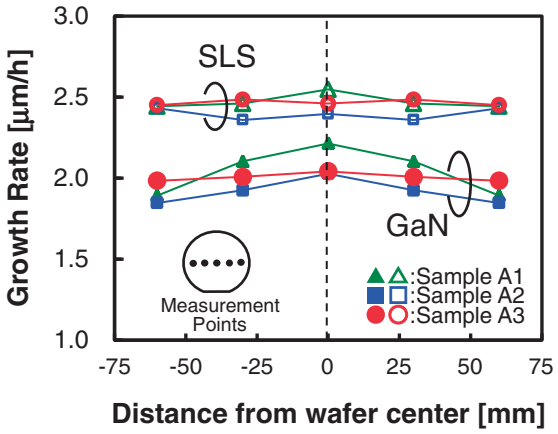

Fig. 3. (Color) Growth rate distributions of SLS and GaN in radial direction.

Table I. Summary of carrier gas flow ratio conditions (top : middle : bottom).

	Gas flow ratio (%)	
	SLS	GaN
Sample A1	40 : 30 : 30	40 : 30 : 30
Sample A2	50 : 25 : 25	50 : 25 : 25
Sample A3	50 : 25 : 25	60 : 20 : 20

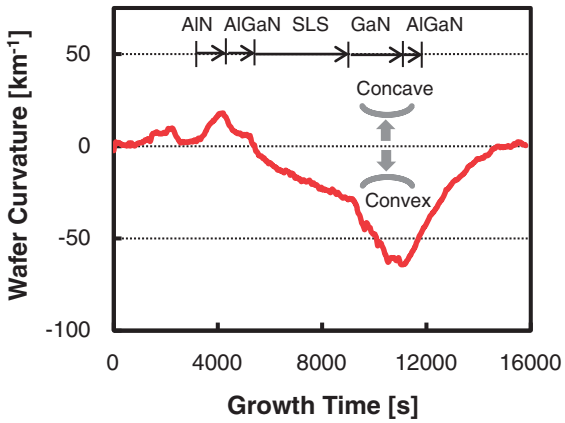

Fig. 4. (Color) Example of typical behavior of wafer curvature during growth of HEMT structure on Si.

also measured by cross-sectional scanning electron microscopy (SEM).

3. Results and Discussion

AlN/Si samples were grown at various rates on the 6″ and 8″ Si substrates at 13 kPa using the above reactors. The AlN thickness was about 200 nm. Figure 2 shows the AlN growth rates obtained at various TMA supply concentrations. If a hazardous parasitic reaction occurs upstream, AlN growth rate should saturate or decrease as TMA supply concentration increases. However, since AlN growth rate extends linearly up to as high as 3.8 μm/h, we can conclude that the gas-phase prereaction is controlled well in these reactors.

To obtain uniform-thickness layers in the entire 6″ wafer, we investigated the effect of the carrier gas flow ratio of the trilayer nozzle. We adopted a strained-layer superlattice (SLS) of AlGaN–AlN pairs and grew a 2.8-μm-thick $Al_{0.21}GaN/AlN/GaN/SLS/Al_{0.5}GaN/AlN$ on 6″ Si substrates using the 7 × 6″ reactor UR25K. The thicknesses of the SLS, GaN, and $Al_{0.21}GaN$ layers were about 1.4 μm, 1.0 μm, and 30 nm, respectively, and the growth rate of SLS was 2.4 μm/h. The growth was performed by changing the ratio of the gas flow introduced from the trilayer nozzle where the total flow rate of the carrier gas was fixed. The three layers of the nozzle were denoted "Top", "Middle", and "Bottom" accordingly, and the condition was defined as "Top : Middle : Bottom". The carrier gas flow ratios for all the layers, such as SLS and GaN, of the three samples are summarized in Table I. Figure 3 shows SLS and GaN growth rate distributions of the three samples in the radial direction. The thickness uniformities of all the layers improved as "Top" flow ratio was increased from sample A1 to sample A3, and the distribution values Δ [(max − min)/average] were ±0.7% for SLS and ±1.4% for GaN. Consequently, the standard deviation of the total thickness of sample A3 was 0.14%. From these results, it is realized that uniform-thickness layers can be achieved by optimizing the gas conditions of the three layers of the trilayer nozzle and by controlling the mass transport at the edge of the wafer.

Figure 4 shows an example of a typical behavior of wafer curvature during the growth of a 3.7-μm-thick HEMT structure on the 8″ Si substrate using our MOCVD tool. First, the Si wafer bowed concavely by tensile strain in AlN growth, and became flatter by compressive strain in AlGaN growth. Compressive stress was introduced in SLS growth and a larger stress was further introduced in GaN growth. During cooling after HEMT growth, the wafer became flatter by the difference in thermal expansion. The wafer temperature reached room temperature within 16000 s after the growth start, and the bow value was approximately 30 μm with a concave shape. Judging from the reciprocal space X-ray mapping on the $(\bar{1}\bar{1}4)$ plane (not shown here), it is thought that the curvature became flat because AlGaN/AlN under SLS, and GaN over SLS were relaxed during cooling. The wafer bows convexly during the growth of the buffer GaN and top AlGaN layers to store compressive strain, which causes a large gradient of surface temperature in a wafer. To obtain a uniform top AlGaN layer, we need to control the gradient of wafer temperature to avoid the effect

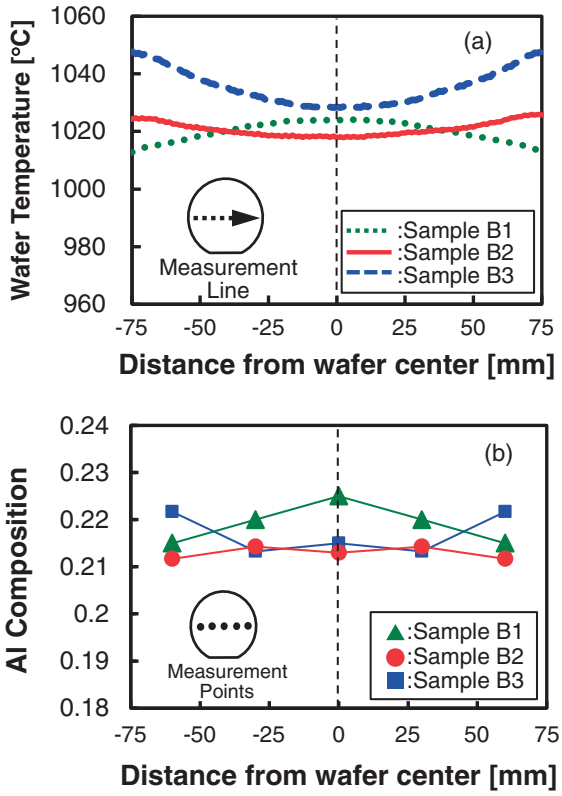

Fig. 5. (Color) Three patterns of wafer temperature profile of samples B1–B3 in radial direction (a) and Al composition distribution of AlGaN samples B1–B3 (b).

of wafer bowing. We investigated the controllability of resistance heaters using a $7 \times 6''$ reactor. Figure 5(a) shows the three patterns of the wafer temperature profile of samples B1–B3 in the radial direction. We can vary the temperature profile by controlling the heater input power of the six zones separately. In samples B1–B3, we have grown $Al_{0.21}GaN/GaN/AlN$ on a $6''$ Si substrate under the heater conditions shown in Fig. 5(a). The thicknesses of the $Al_{0.21}GaN$ and GaN layers were 35 nm and 0.8 μm, respectively. Figure 5(b) shows the Al composition distributions of the AlGaN samples. The Al composition at the substrate perimeter became relatively high when the temperature at the substrate perimeter was high, and vice versa. The Al composition of sample B2 with the most uniform distribution was 0.21 ± 0.002. By using these results, the uniform distribution of the Al composition of AlGaN can be achieved by controlling heater power balance.

By the same method as that using the $7 \times 6''$ reactor UR25K, we have attempted to grow a 3.7-μm-thick $Al_{0.23}GaN/AlN/GaN/SLS/Al_{0.5}GaN/AlN$ HEMT on six $8''$ Si substrates using the $6 \times 8''$ reactor UR26K. The first growth conditions were decided using our own scale-up model from the conditions in the $7 \times 6''$ reactor. Crack-free and smooth surfaces were obtained in the $8''$ wafers. The thicknesses of the SLS and GaN layers were about 2.5 and 0.6 μm, respectively, and the growth rate of SLS was as high as 2.8 μm/h. Figure 6 shows the total thickness mapping data of all six $8''$ wafers. The standard deviations of the thickness were less than 2.0% on wafer and 0.31% wafer to wafer. The typical Al composition of the top AlGaN layer

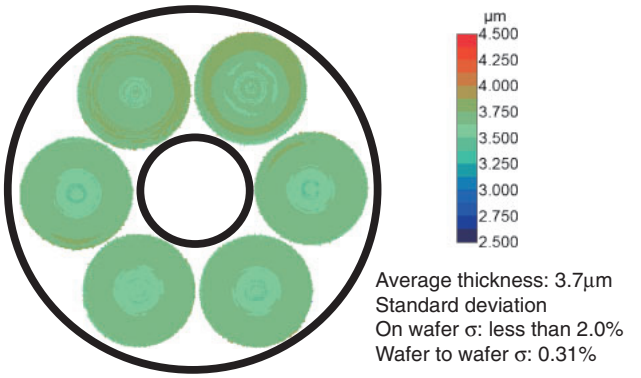

Fig. 6. (Color) Total thickness mapping data of all six $8''$ HEMT wafers.

was 0.23 ± 0.006 on wafer, and the standard deviation was 0.58% wafer to wafer. It is possible to improve the thickness and Al composition uniformities by optimizing gas flow conditions and heater power balance. The electrical properties of the $8''$ HEMT samples were investigated by Van der Pauw measurement. The typical electron mobility was 1670 $cm^2 \cdot V^{-1} \cdot s^{-1}$ at a sheet carrier density of 1.11×10^{13} cm^{-2}. These electrical properties are comparable to the reported data for the $8''$ wafer.[24] Details of the HEMT performance will be reported elsewhere in the near future.

4. Summary

In the growth of a 2.8-μm-thick $Al_{0.21}GaN/AlN/GaN/SLS/Al_{0.5}GaN/AlN$ on $6''$ Si substrates using a $7 \times 6''$ reactor, it was shown that uniform-thickness layers can be achieved by optimizing the gas flow conditions of a trilayer nozzle. The growth rate of SLS was 2.4 μm/h. A uniform distribution of the Al composition of AlGaN can be achieved by controlling heater input power balance. By using our own scale-up model of the growth conditions from those for the $7 \times 6''$ reactor, we have grown a 3.7-μm-thick $Al_{0.23}GaN/AlN/GaN/SLS/Al_{0.5}GaN/AlN$ HEMT on six $8''$ Si substrates using a $6 \times 8''$ reactor. The growth rate of SLS was 2.8 μm/h. The standard deviations of the total thickness were less than 2.0% on wafer and 0.31% wafer to wafer. The typical Al composition of the top AlGaN layer was 0.23 ± 0.006 on wafer, and the standard deviation was 0.58% wafer to wafer. The typical electron mobility was 1670 $cm^2 \cdot V^{-1} \cdot s^{-1}$ at a sheet carrier density of 1.11×10^{13} cm^{-2}. In this study, the possibility of the mass production of HEMTs on $8''$ Si substrates using a $6 \times 8''$ reactor was shown.

1) J. Chen, S. Zhang, B. Zhang, J. Zhu, G. Feng, L. Duan, Y. Wang, H. Yang, and W. Zheng: Sci. China, Ser. E **46** (2003) 620.
2) A. E. Wickenden, D. D. Koleske, R. L. Henry, R. J. Gorman, M. E. Twigg, M. Fatemi, J. A. Freitas, Jr., and W. J. Moore: J. Electron. Mater. **29** (2000) 21.
3) A. E. Wickenden, D. D. Koleske, R. L. Henry, M. E. Twigg, and M. Fatemi: J. Cryst. Growth **260** (2004) 54.
4) D. Zhu, C. McAleese, K. K. McLaughlin, M. Häberlen, C. O. Salcianu, E. J. Thrush, M. J. Kappersa, W. A. Phillips, P. Lane, D. J. Wallis, T. Martin, M. Astles, S. Thomas, A. Pakes, M. Heuken, and C. J. Humphreys: Proc. SPIE **7231** (2009) 723118.
5) A. Dadgar, M. Poschenrieder, J. Bläsing, O. Contreras, F. Bertram, T. Riemann, A. Reiher, M. Kunze, I. Daumiller, A. Krtschil, A. Diez, A.

Kaluza, A. Modlich, M. Kamp, J. Christen, F. A. Ponce, E. Kohn, and A. Krost: J. Cryst. Growth **248** (2003) 556.
6) T. Egawa, T. Moku, H. Ishikawa, K. Ohtsuka, and T. Jimbo: Jpn. J. Appl. Phys. **41** (2002) L663.
7) J. Selvaraj, S. L. Selvaraj, and T. Egawa: Jpn. J. Appl. Phys. **48** (2009) 121002.
8) S. Tripathy, V. K. X. Lin, S. B. Dolmanan, J. P. Y. Tan, R. S. Kajen, L. K. Bera, S. L. Teo, M. K. Kumar, S. Arulkumaran, G. I. Ng, S. Vicknesh, S. Todd, W. Z. Wang, G. Q. Lo, H. Li, D. Lee, and S. Han: Appl. Phys. Lett. **101** (2012) 082110.
9) J. Y. Kim, Y. Tak, J. Kim, H. G. Hong, S. Chae, J. W. Lee, H. Choi, Y. Park, U. I. Chung, J. R. Kim, and J. I. Shim: Proc. SPIE **8262** (2012) 82621D.
10) Y. Uemoto, T. Morita, A. Ikoshi, H. Umeda, H. Matsuo, J. Shimizu, M. Hikita, M. Yanagihara, T. Ueda, T. Tanaka, and D. Ueda: IEDM Tech. Dig., 2009, p. 1.
11) Y. Wu, M. Jacob-Mitos, M. L. Moore, and S. Heikman: IEEE Electron Device Lett. **29** (2008) 824.
12) N. Ikeda, Y. Niiyama, H. Kambayashi, Y. Satoh, T. Nomura, S. Kato, and S. Yoshida: Proc. IEEE **98** (2010) 1151.
13) S. Arulkumaran, S. Vicknesh, N. G. Ing, S. L. Selvaraj, and T. Egawa: Appl. Phys. Express **4** (2011) 084101.
14) C. Roder, S. Einfeldt, S. Figge, and D. Hommel: Phys. Rev. B **72** (2005) 085218.
15) A. Krost, A. Dadgar, F. Schulze, J. Bläsing, G. Strassburger, R. Clos, A. Diez, P. Veit, T. Hempel, and J. Christen: J. Cryst. Growth **275** (2005) 209.
16) K. Matsumoto, A. Ubukata, K. Ikenaga, K. Naito, J. Yamamoto, Y. Yano, T. Tabuchi, A. Yamaguchi, Y. Ban, and K. Uchiyama: Proc. SPIE **8262** (2012) 826202.
17) H. Tokunaga, H. Tan, Y. Inaishi, T. Arai, A. Yamaguchi, and J. Hidaka: J. Cryst. Growth **221** (2000) 616.
18) H. Tokunaga, Y. Fukuda, A. Ubukata, K. Ikenaga, Y. Inaishi, T. Orita, S. Hasaka, Y. Kitamura, A. Yamaguchi, S. Koseki, K. Uematsu, N. Tomita, N. Akutsu, and K. Matsumoto: Phys. Status Solidi C **5** (2008) 3017.
19) A. Ubukata, K. Ikenaga, N. Akutsu, K. Matsumoto, T. Yamazaki, and T. Egawa: J. Cryst. Growth **298** (2007) 198.
20) K. Uchida, H. Tokunaga, Y. Inaishi, N. Akutsu, K. Matsumoto, T. Itoh, T. Egawa, T. Jimbo, and M. Umeno: MRS Proc. **449** (1996) 129.
21) K. Matsumoto and A. Tachibana: J. Cryst. Growth **272** (2004) 360.
22) T. Arai, J. Hidaka, H. Tokunaga, and K. Matsumoto: J. Cryst. Growth **170** (1997) 88.
23) K. Matsumoto, T. Arai, and H. Tokunaga: Vacuum **51** (1998) 699.
24) K. Cheng, H. Liang, M. V. Hove, K. Geens, B. D. Jaeger, P. Srivastava, X. Kang, P. Favia, H. Bender, S. Decoutere, J. Dekoster, J. I. A. Borniquel, S. W. Jun, and H. Chung: Appl. Phys. Express **5** (2012) 011002.